



Simulating the effects of light intensity and carbonate system composition on particulate organic and inorganic carbon production in *Emiliana huxleyi*



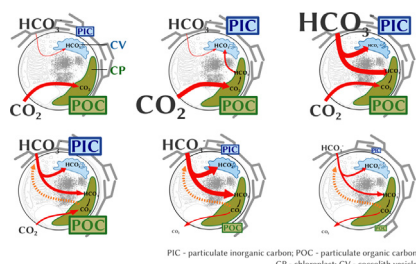
Lena-Maria Holtz*, Dieter Wolf-Gladrow, Silke Thoms

Alfred-Wegener-Institut, Helmholtz-Zentrum für Polar- und Meeresforschung, Am Handelshafen 12, 27570 Bremerhaven, Germany

HIGHLIGHTS

- A numerical cell model is developed for *Emiliana huxleyi*.
- Cellular C fluxes are examined for different light and carbonate system conditions.
- PIC and POC production rates can be explained mechanistically.

GRAPHICAL ABSTRACT



ARTICLE INFO

Article history:

Received 8 August 2014

Received in revised form

20 February 2015

Accepted 25 February 2015

Available online 5 March 2015

Keywords:

CO₂/carbon uptake

Coccolithophores

Marine carbon cycle

Phytoplankton

ABSTRACT

Coccolithophores play an important role in the marine carbon cycle. Variations in light intensity and external carbonate system composition alter intracellular carbon fluxes and therewith the production rates of particulate organic and inorganic carbon. Aiming to find a mechanistic explanation for the interrelation between dissolved inorganic carbon fluxes and particulate carbon production rates, we develop a numerical cell model for *Emiliana huxleyi*, one of the most abundant coccolithophore species. The model consists of four cellular compartments, for each of which the carbonate system is resolved dynamically. The compartments are connected to each other and to the external medium via substrate fluxes across the compartment-confining membranes. By means of the model we are able to explain several pattern observed in particulate organic and inorganic carbon production rates for different strains and under different acclimation conditions. Particulate organic and inorganic carbon production rates for instance decrease at very low external CO₂ concentrations. Our model suggests that this effect is caused mainly by reduced HCO₃⁻ uptake rates, not by CO₂ limitation. The often observed decrease in particulate inorganic carbon production rates under Ocean Acidification is explained by a down-regulation of cellular HCO₃⁻ uptake.

© 2015 The Authors. Published by Elsevier Ltd. This is an open access article under the CC BY-NC-ND license (<http://creativecommons.org/licenses/by-nc-nd/4.0/>).

Abbreviation: Ω, calcite saturation level; CA, carbonic anhydrase; CCM, CO₂/carbon concentrating mechanism; CV, calcification/coccolith vesicle; DIC, dissolved inorganic carbon, i.e. sum of CO₂, H₂CO₃, HCO₃⁻, and CO₃²⁻; PIC, particulate inorganic carbon, here calcite; POC, particulate organic carbon; RubisCO, Ribulose-1,5-bisphosphate-Carboxylase/Oxygenase

* Corresponding author. Tel.: +49 471 4831 2093.

E-mail address: lena-maria.holtz@awi.de (L.-M. Holtz).

<http://dx.doi.org/10.1016/j.jtbi.2015.02.024>

0022-5193/© 2015 The Authors. Published by Elsevier Ltd. This is an open access article under the CC BY-NC-ND license (<http://creativecommons.org/licenses/by-nc-nd/4.0/>).

1. Introduction

Coccolithophores contribute up to 10% to net marine primary production which in total accounts for around 50 Pg carbon per year (Poulton et al., 2007; Field et al., 1998). Together with foraminifera, they belong to the main pelagic calcium carbonate producers that precipitate around 2.4 Pg carbon per year (Milliman, 1993). Calcium

carbonate may act as an important ballast mineral in the biological carbon pump (Armstrong et al., 2002; Schmidt et al., 2014). In contrast to particulate organic carbon (POC) production which shifts the carbonate system of the surface ocean towards higher pH values and hence an uptake of atmospheric CO₂, particulate inorganic carbon (PIC) production has the opposite effect due to the concurrent reduction in total alkalinity. The production rates of POC and PIC are dependent on the abiotic growth conditions such as the composition of the external carbonate system, light intensities, temperatures, and nutrient availabilities (e.g. Hoppe et al., 2011; Sett et al., 2014; Rouco et al., 2013).

Anthropogenic CO₂ emissions (in 2011: ca. 9 Pg C a⁻¹, Peters et al., 2011) alter the composition of the sea surface carbonate system: the concentration of CO₂ rises, while the concentration of CO₃²⁻ and the pH drop ('Ocean Acidification'). Increasing atmospheric CO₂ concentrations further go along with rising sea surface temperatures (increase of 0.3–0.5 °C from 1960 to 2005, Solomon et al., 2007) which can lead to stronger stratification and thus a shoaling of the upper surface layer, especially in high latitudes. Besides lower nutrient availabilities these changes further imply higher integrated light intensities in the upper mixed water layer.

As coccolithophores constitute an essential component of the global marine carbon cycle which they impact quite differently depending on the PIC and POC production rates they exhibit, it is important to understand how these rates are influenced by abiotic conditions. After more than five decades of intensive research, the cellular regulation of PIC and POC production rates still remains unresolved (reviews: Paasche, 2002; Raven and Crawford, 2012). Light intensity and the concentrations of CO₂ and HCO₃⁻ constitute crucial abiotic factors that will change in the future surface ocean. In this paper, we will thus examine how these abiotic factors affect internal carbon fluxes and therewith PIC and POC production rates of *Emiliania huxleyi*, one of the most abundant and best-studied coccolithophore species.

Based on experimental evidence, the numerical model of Holtz et al. (2015) is extended. Particulate organic and inorganic carbon production rates are calculated for different light intensities and carbonate system compositions and successfully compared to the data sets published by Zondervan et al. (2002)/Rost et al. (2002) (strain PML B92/11), Langer et al. (2009) (strains RCC1212, RCC1216, RCC1238, and RCC1256), Hoppe et al. (2011) (strains NZEH/PLY M219 and RCC1256), Bach et al. (2013), and Sett et al. (2014) (both strain PML B92/11).

2. Model

2.1. Concept

We hypothesise that phytoplankton cells prefer CO₂ over HCO₃⁻ as inorganic carbon source for POC production. In comparison to diffusive CO₂ uptake which does not require high cellular energy investments, HCO₃⁻ uptake is more expensive for the cell. One reason hereof is

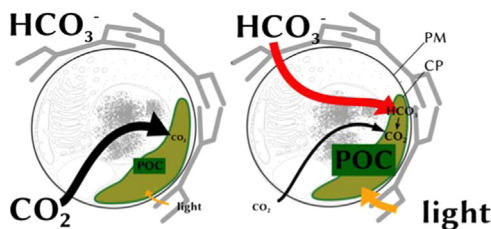


Fig. 1. Hypothesis of Holtz et al. (2015): at high light intensities and low CO₂ concentrations (right), the carbon demand of photosynthesis is accomplished by HCO₃⁻ via increasing HCO₃⁻ uptake. CP, chloroplast; PM, plasma membrane. Illustration includes part that was redrawn after van der Wal et al. (1983).

that HCO₃⁻ is surrounded by a hydrate shell that probably has to be stripped off (an energy-requiring process) in order to traverse HCO₃⁻-specific channel or transporter proteins (Gouaux and MacKinnon, 2005). Furthermore, the inner face of the plasma membrane is charged negatively. This negative charging has to be overcome by HCO₃⁻ when entering the cell. Whether energisation is needed for this process depends on the electrochemical potential difference of HCO₃⁻ across the plasma membrane, i.e. the sum of the electrical and the chemical potential difference. The electrical potential is determined by the distribution of charges across the membrane and the chemical by the distribution of concentrations. Since neither the ion distributions to particular compartments nor the functionality of the implemented ion transport systems is known in sufficient detail, we restrict model calculations to substrate concentrations, i.e. to the chemical gradients. Last but not least, the principle of charge neutrality has to be ensured when trans-membrane fluxes of ions are considered (Wolf-Gladrow et al., 2007), i.e. the overall net charging that passes the complete compartment-confining membrane has to be zero. It follows that the energy requirement of trans-membrane HCO₃⁻ fluxes is furthermore dependent on the electrochemical potential differences of co- or antiported substrates.

For different diatom species, Hopkinson et al. (2011) determined very high passive CO₂ (cf. Uehlein et al., 2008 for higher plants) and negligibly low HCO₃⁻ fluxes across the plasma membrane which supports our hypothesis. High diffusive CO₂ uptake rates, however, cannot simply be effected by high CO₂ permeability coefficients, they further rely on CO₂ concentration gradients across the plasma membrane that drive CO₂ into the cell. Due to the low CO₂ concentrations that usually predominate surface waters, CO₂ concentration gradients directing into the cell may well constitute the limiting factor for diffusive CO₂ uptake. By means of a previous cell model (Holtz et al., 2015), we showed that photosynthetic carbon fixation rates can exceed diffusive CO₂ influx rates at high light intensities (≡ high CO₂ fixation rates) or low external CO₂ concentrations. It was thus suggested that when diffusive CO₂ uptake cannot cover the carbon demand of photosynthesis, external HCO₃⁻ becomes the alternative carbon source for POC production (cf. Fig. 1).

Several experimental findings support this switch from CO₂ to HCO₃⁻ usage: Rost et al. (2002) showed that the biomass of cells that grow fast and at low CO₂ concentrations contains more ¹³C than the biomass of cells that grow slowly and at high CO₂ concentrations. The authors attribute the heavier biomass composition of the fast growing cells to higher HCO₃⁻ usage for POC production, because HCO₃⁻ exhibits higher ¹³C:¹²C ratios than CO₂ in equilibrium (Zeebe and Wolf-Gladrow, 2001). By means of ¹⁴C disequilibrium assays, Kottmeier et al. (2014) showed that relative HCO₃⁻ usage for POC production increases under low external CO₂ concentrations. Bach et al. (2013) found the 'anion exchanger like 1' (AEL1) upregulated under low DIC (dissolved inorganic carbon = sum of all inorganic carbon species) concentrations in *E. huxleyi*. AEL1 is thought to be involved in cellular HCO₃⁻ uptake. It is thus feasible that AEL1, i.e. cellular HCO₃⁻ uptake, is upregulated to overcome the shortcoming in diffusive CO₂ provision to Ribulose-1,5-bisphosphate-Carboxylase/Oxygenase (RubisCO).

2.2. Implementation

The cell model comprises four compartments (Fig. 2), namely the cytosol (CS), the coccolith vesicle (CV), the chloroplast stroma (CPs), and the thylakoid/pyrenoid complex (TP). Each compartment contains CO₂, HCO₃⁻, CO₃²⁻, OH⁻, and H⁺ that react with each other (cf. Section 2.2.1). The four compartments are connected to each other as well as to the external medium/seawater (SW) via substrate fluxes across the compartment-confining membranes (cf. Sections 2.2.2 and 2.2.5). Inside CV and TP, carbon is fixed into PIC and POC, respectively

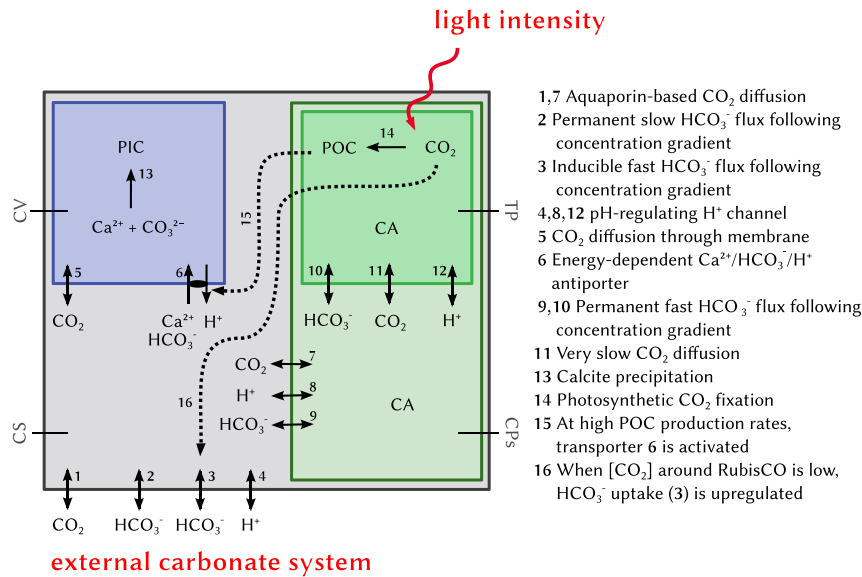


Fig. 2. Cell model set-up. Arrows with solid lines indicate substrate fluxes across membranes. Arrows with dotted lines indicate regulating mechanisms. External carbonate system (especially $[\text{CO}_2]$ and $[\text{HCO}_3^-]$) and light intensities constitute the model forcings. CA, carbonic anhydrase; CPs, chloroplast stroma; CS, cytosol; TP, thylakoid/pyrenoid complex. Inside the CS, the CPs, and the TP, pH values are strictly regulated: $\text{pH}_{\text{CS}} = 7$, $\text{pH}_{\text{CPs}}(\text{illumination}) = 8$, $\text{pH}_{\text{TP}}(\text{illumination}) = 5$, $\text{pH}_{\text{CPs}}(\text{darkness}) = 7$, $\text{pH}_{\text{TP}}(\text{darkness}) = 7$.

Table 1

External (seawater, SW) carbonate systems that force the model. In one approach (carbonate systems 1), dissolved inorganic carbon is set to $2.052 \text{ mmol m}^{-3}$ and $[\text{CO}_2]$ is adjusted by varying the pH value. These carbonate systems are hence in equilibrium. In another approach (carbonate systems 2), pH and $[\text{HCO}_3^-]$ are set constant, while the CO_2 concentration varies from 0.5 to 44.8 mmol m^{-3} . The latter carbonate systems are thus out of equilibrium and are used exclusively to examine the influence of external $[\text{HCO}_3^-]$ on the model outputs which is done by comparing the outputs generated on basis of carbonate systems 1, where $[\text{HCO}_3^-]$ is variable, to those generated on basis of carbonate systems 2, where $[\text{HCO}_3^-]$ is set constant. Temperature = 15°C , salinity = 32.

Carbonate systems 1			Carbonate systems 2		
pH	$[\text{CO}_2]^{\text{SW}}$ (mmol m^{-3})	$[\text{HCO}_3^-]^{\text{SW}}$ (mmol m^{-3})	pH	$[\text{CO}_2]^{\text{SW}}$ (mmol m^{-3})	$[\text{HCO}_3^-]^{\text{SW}}$ (mmol m^{-3})
9.2	0.5	906	8.2	0.5	2000
8.6	3.6	1555	8.2	3.6	2000
8.2	10.5	1813	8.2	10.5	2000
8.0	17.3	1885	8.2	17.3	2000
7.8	28.0	1928	8.2	28.0	2000
7.7	35.5	1940	8.2	35.4	2000
7.6	44.8	1947	8.2	44.8	2000

(cf. Sections 2.2.6 and 2.2.7). One key feature of the model is that CO_2 can be accumulated around RubisCO ('carbon/ CO_2 concentrating mechanism', CCM) without pumping inorganic carbon species against their concentration gradients. A detailed description of the chloroplast-based CCM and justifications for its application to *E. huxleyi* are given in the model description of Holtz et al. (2015). Four new important features in comparison to this previous model (Holtz et al., 2015) are that (1) besides CO_2 , HCO_3^- can enter the chloroplast, (2) the potential for cellular HCO_3^- uptake is upregulated when the CO_2 concentration around RubisCO falls below a critical threshold, (3) active transport processes across the CV membrane are made dependent on the net POC production rate as a rough estimate of respirational processes that provide energy equivalents, and (4) POC as well as PIC production rates are not set to a predefined value but calculated by the model. The model is forced by different light intensities and different external carbonate system compositions.

Parameter values used in the following are listed and explained in Tables 1 (external carbonate system), 2 (rate constants (k) for

Table 2

Rate constants of the carbonate systems after Zeebe and Wolf-Gladrow (2001). Temperature is 15°C , the salinity in seawater (SW) 32 and 30 within the cell.

Rate constant (unit)	Values	
	SW	Cell
k_{+1} (s^{-1})	14.2×10^{-3}	14.2×10^{-3}
k_{-1} ($\text{L mol}^{-1} \text{s}^{-1}$)	12.7×10^3	12.9×10^3
k_{+4} ($\text{L mol}^{-1} \text{s}^{-1}$)	2.86×10^3	2.86×10^3
k_{-4} (s^{-1})	6.06×10^{-5}	5.96×10^{-5}
$k_{+5}^{\text{H}^+}$ ($\text{L mol}^{-1} \text{s}^{-1}$)	4.88×10^{10}	4.89×10^{10}
$k_{-5}^{\text{H}^+}$ (s^{-1})	37.3	35.5
$k_{+5}^{\text{OH}^-}$ ($\text{L mol}^{-1} \text{s}^{-1}$)	5.86×10^9	5.87×10^9
$k_{-5}^{\text{OH}^-}$ (s^{-1})	1.82×10^5	1.85×10^5
k_{+6} ($\text{mol L}^{-1} \text{s}^{-1}$)	1.43×10^{-3}	1.43×10^{-3}
k_{-6} ($\text{L mol}^{-1} \text{s}^{-1}$)	6.04×10^{10}	6.27×10^{10}

carbonate system), 3 (compartment volumes (V) and surface areas (A)), and 4 (other parameters). Units used in the equations are based on mol, m, and h, unless stated otherwise.

2.2.1. Carbonate system

The carbonate system (CO_2 , HCO_3^- , CO_3^{2-} , H^+ , and OH^- , cf. Eqs. (1)–(5)) is resolved dynamically for all four compartments (after Zeebe and Wolf-Gladrow, 2001, temperature = 15°C , salinity in seawater = 32, salinity inside cell = 30).





The corresponding net reaction rates are denoted according to the notation of rate constants and describe the reactions (1)–(5) from right to left.

$$R_1 = -k_{+1} \cdot [\text{CO}_2] + k_{-1} \cdot [\text{H}^+] \cdot [\text{HCO}_3^-] \quad (6)$$

$$R_4 = -k_{+4} \cdot [\text{OH}^-] \cdot [\text{CO}_2] + k_{-4} \cdot [\text{HCO}_3^-] \quad (7)$$

$$R_5^{\text{H}^+} = -k_{+5}^{\text{H}^+} \cdot [\text{H}^+] \cdot [\text{CO}_3^{2-}] + k_{-5}^{\text{H}^+} \cdot [\text{HCO}_3^-] \quad (8)$$

$$R_5^{\text{OH}^-} = -k_{+5}^{\text{OH}^-} \cdot [\text{OH}^-] \cdot [\text{HCO}_3^-] + k_{-5}^{\text{OH}^-} \cdot [\text{CO}_3^{2-}] \quad (9)$$

Table 3

Morphological parameter values of the four compartments. CP, chloroplast; CPs, chloroplast stroma; CS, cytosol; CV, coccolith vesicle; PM, plasma membrane; TP, thylakoid/pyrenoid complex.

Parameter	Description	Value
V^{CS}	Volume CS	$16.1 \times 10^{-18} \text{ m}^3$
A^{CS}	PM amount	$78.5 \times 10^{-12} \text{ m}^2$
V^{CV}	Volume CV	$1.6 \times 10^{-18} \text{ m}^3$
A^{CV}	CV membrane amount	$16.8 \times 10^{-12} \text{ m}^2$
V^{CPs}	Volume CPs	$22.6 \times 10^{-18} \text{ m}^3$
A^{CP}	Membrane surrounding CP	$64.1 \times 10^{-12} \text{ m}^2$
V^{TP}	Volume TP	$5.7 \times 10^{-18} \text{ m}^3$
A^{TP}	Membrane surrounding TP	$37 \times 10^{-12} \text{ m}^2$

Table 4

Parameter description and values. (no.) is the number allocated in Fig. 2. CPm, chloroplast envelope; CS, cytosol; CV, coccolith vesicle; CVm, membrane surrounding CV; PM, plasma membrane; TP, thylakoid/pyrenoid complex; TPm, membrane surrounding TP.

Parameter (no.)	Description	value
$\gamma_{\text{CO}_2}^{\text{PM}}$ (1)	Permeability coefficient of PM to CO_2	0.54 m h^{-1} Hopkinson et al. (2011)
$\gamma_{\text{CO}_2}^{\text{CVm}}$ (5)	Permeability coefficient of CVm to CO_2	0.02 m h^{-1} Prasad et al. (1998)
$\gamma_{\text{CO}_2}^{\text{CPm}}$ (7)	Permeability coefficient of CPm to CO_2	$0.54/3 \text{ m h}^{-1}$, after Hopkinson et al. (2011), Thoms et al. (2001)
$\gamma_{\text{CO}_2}^{\text{TPm}}$ (11)	Permeability coefficient of TPm to CO_2	0.01 m h^{-1}
$\gamma_{\text{HCO}_3^-}^{\text{PM,p}}$ (2)	Channel-mediated permeability of permanently opened HCO_3^- uptake system in PM	0 m h^{-1} , after Hopkinson et al. (2011)
$\gamma_{\text{HCO}_3^-}^{\text{PM,i}}$ (3)	Channel-mediated permeability of inducible HCO_3^- uptake system in PM	$25 \times 10^{-3} \text{ m h}^{-1}$
$\gamma_{\text{HCO}_3^-}^{\text{CPm}}$ (9)	Channel-mediated permeability of CPm	$17 \times 10^{-4} \text{ m h}^{-1}$
$\gamma_{\text{HCO}_3^-}^{\text{TPm}}$ (10)	Channel-mediated permeability of TPm	$25 \times 10^{-3} \text{ m h}^{-1}$
$[\text{Ca}^{2+}]^{\text{CS}}$ (6)	$[\text{Ca}^{2+}]$ inside CS	$0.1 \times 10^{-3} \text{ mol m}^{-3}$ Brownlee et al. (1995)
$[\text{H}^+]_{\text{thres,PM}}$ (4)	$[\text{H}^+]$ to be reached inside CS	$1.022 \times 10^{-4} \text{ mol m}^{-3}$ Anning et al. (1996)
$[\text{H}^+]_{\text{thres,CPm}}$ (8)	$[\text{H}^+]$ to be reached inside CPs during illumination	$1.022 \times 10^{-5} \text{ mol m}^{-3}$, after Heldt et al. (1973)
$[\text{H}^+]_{\text{thres,CPm}}^{\text{D}}$ (8)	$[\text{H}^+]$ to be reached inside CPs during darkness	$1.022 \times 10^{-4} \text{ mol m}^{-3}$, after Heldt et al. (1973)
$[\text{H}^+]_{\text{thres,TPm}}$ (12)	$[\text{H}^+]$ to be reached inside TP during illumination	$1.022 \times 10^{-2} \text{ mol m}^{-3}$, after Heldt et al. (1973)
$[\text{H}^+]_{\text{thres,TPm}}^{\text{D}}$ (12)	$[\text{H}^+]$ to be reached inside TP during darkness	$1.022 \times 10^{-4} \text{ mol m}^{-3}$, after Heldt et al. (1973)
$[\text{HCO}_3^-]_{\text{thres}}$ (6)	$[\text{HCO}_3^-]$ below which $\text{Ca}^{2+}/\text{HCO}_3^-/\text{H}^+$ transporter is substrate-limited	0.6 mol m^{-3}
k_f (13)	Calcite precipitation related rate constant	$10^{-9} \text{ mol m}^{-3} \text{ h}^{-1}$ Zuddas and Mucci (1994)
K_m^{Rub} (14 and 16)	Half-saturation constant of RubisCO to CO_2	$72 \times 10^{-3} \text{ mol m}^{-3}$ Boller et al. (2011)
L_{cv} (14)	Conversion factor from amol s^{-1} to mol h^{-1}	$36 \times 10^{-16} \text{ s h}^{-1} \text{ mol amol}^{-1}$
n (13)	Calcite precipitation related parameter	2.35 Zuddas and Mucci (1994)
$R_{\text{CaHCOH}}^{\text{Ca}^{2+}}$ (6)	Max. flux of Ca^{2+} , HCO_3^- , and H^+ across CV membrane	$1.96 \times 10^{-13} \text{ mol h}^{-1}$
$R_{\text{H}^+}^{\text{max}}$ (4, 8, and 12)	Maximum rate by which $[\text{H}^+]$ changes	$600 \text{ mol m}^{-2} \text{ h}^{-1}$
R_{PSmin} (6)	Min. photosynthetic C fixation rate above which $\text{Ca}^{2+}/\text{HCO}_3^-/\text{H}^+$ transporter can be active	$1731 \text{ mol m}^{-3} \text{ h}^{-1}$
R_{PSmax} (6)	Max. photosynthetic C fixation rate	$31497 \text{ mol m}^{-3} \text{ h}^{-1}$

$$R_6 = -k_{+6} + k_{-6} \cdot [\text{H}^+] \cdot [\text{OH}^-]. \quad (10)$$

For the chloroplast stroma and the thylakoid lumen, carbonic anhydrase activity is assumed, i.e. R_1 (Eq. (6)) is multiplied by 10^4 (Supuran and Scozzafava, 2007).

2.2.2. Carbon dioxide fluxes (1, 5, 7, and 11 in Fig. 2)

Carbon dioxide diffuses across membranes (here: mem) from one compartment (here: com b) into another compartment (here: com a) following its concentration gradient. The rate by which the CO_2 concentration in compartment com a changes is $R_{\text{CO}_2, \text{mem}}^{\text{com a}}$.

$$R_{\text{CO}_2, \text{mem}}^{\text{com a}} = \gamma_{\text{CO}_2}^{\text{mem}} \cdot \frac{A^{\text{com a}}}{V^{\text{com a}}} \cdot ([\text{CO}_2]^{\text{com b}} - [\text{CO}_2]^{\text{com a}}) \quad (11)$$

$A^{\text{com a}}$ and $V^{\text{com a}}$ stand for surface area and volume of compartment com a (cf. Table 3), and $\gamma_{\text{CO}_2, \text{mem}}$ gives the permeability coefficient of membrane mem to CO_2 (cf. Table 4).

2.2.3. Bicarbonate fluxes across plasma membrane, chloroplast envelope, and thylakoid/pyrenoid complex (2, 3, 9, and 10 plus 16 in Fig. 2)

With the exception of the HCO_3^- flux across the CV membrane (6 in Fig. 2, Section 2.2.5) HCO_3^- fluxes follow their concentration gradients in this model.

$$R_{\text{HCO}_3^-, \text{mem}}^{\text{com a}} = \gamma_{\text{HCO}_3^-}^{\text{mem}} \cdot \frac{A^{\text{com a}}}{V^{\text{com a}}} \cdot ([\text{HCO}_3^-]^{\text{com b}} - [\text{HCO}_3^-]^{\text{com a}}) \cdot \text{fun}_{\text{HCO}_3^-}^{\text{CO}_2} \quad (12)$$

Thus, depending on the concentration gradient across membrane mem, HCO_3^- can enter or leave compartments com a and com b in our model. For the plasma membrane a dimensionless regulation factor is introduced ($\text{fun}_{\text{HCO}_3^-}^{\text{CO}_2}$, 16 in Fig. 2), which regulates the

activation of the HCO_3^- channel (flux **3**) depending on the saturation state of RubisCO. This HCO_3^- channel is implemented for the anion exchanger like 1 (AE1) by

$$\text{fun}_{\text{HCO}_3^-}^{\text{CO}_2} = \begin{cases} \frac{1}{2} \cdot \tanh \left[3.5 \cdot \left(0.6 \cdot K_m^{\text{Rub}} - [\text{CO}_2]^{\text{TP}} \right) \right] + \frac{1}{2} & \text{in the light} \\ 0 & \text{at darkness} \end{cases} \quad (13)$$

where K_m^{Rub} , the half saturation constant of RubisCO towards CO_2 , is given in mol m^{-3} . In case of fluxes **2**, **9**, and **10**, $\text{fun}_{\text{HCO}_3^-}^{\text{CO}_2}$ is set to 1.

2.2.4. pH-regulating H^+ fluxes (**4**, **8**, and **12** in Fig. 2)

We assume that internal pH homeostasis can be maintained in cells that grow under acclimation at a pH value above 7.6. In this case, the pH values of the *in silico* cytosol, the chloroplast stroma, and the thylakoid/pyrenoid complex are strictly regulated via H^+ fluxes between cellular compartments and the external medium in our model. The rate by which the H^+ concentration in compartment com a changes is

$$R_{\text{H}^+}^{\text{com a, mem}} = \text{fun}_{\text{H}^+} \cdot R_{\text{H}^+}^{\text{max}} \cdot \frac{A^{\text{com a}}}{V^{\text{com a}}} \quad (14)$$

fun_{H^+} is a cut-off function that determines strength and direction of the H^+ flux depending on the prevailing H^+ concentration.

$$\text{fun}_{\text{H}^+} = \tanh \left([\text{H}^+]^{\text{com a}} - [\text{H}^+]^{\text{thresh, com a}} \right) \quad (15)$$

The pH values inside chloroplast stroma and thylakoid/pyrenoid complex vary over the light:dark cycle due to the on- and offset of the photosynthetic light reaction which drives and energises the transport of H^+ into the thylakoid lumen during illumination (Heldt et al., 1973).

2.2.5. Calcium ion and HCO_3^- uptake into the cocolith vesicle (**6** in Fig. 2)

Bicarbonate ions enter the CV together with Ca^{2+} and in antiport against H^+ (cf. Holtz et al., 2015).

$$R_{\text{CaHCOH, CVm}}^{\text{Ca}^{2+}} = \frac{R_{\text{CaHCOH}}^{\text{Ca}^{2+}}}{V_{\text{CV}}} \cdot \text{fun}_{\text{CaHCOH}}^{\text{Ca}^{2+}} \cdot \text{fun}_{\text{CaHCOH}}^{\text{HCO}_3^-} \cdot \text{fun}_{\text{CaHCOH}}^{\text{ener}} \quad (16)$$

The activity of this ' $\text{Ca}^{2+}/\text{HCO}_3^-/\text{H}^+$ transporter' (stoichiometry: 1:1:–1) is influenced by the Ca^{2+} concentrations inside the cytosol (parameterised cf. Berridge et al., 2000) and the CV (variable, cf. Eq. (17)), the HCO_3^- concentration inside the cytosol (cf. Eq. (18)), and

the availability of energy equivalents (cf. Eq. (19)).

$$\text{fun}_{\text{CaHCOH}}^{\text{Ca}^{2+}} = \frac{1}{2} \cdot \tanh \left[100 \cdot \left(10^5 \cdot [\text{Ca}^{2+}]^{\text{CS}} - [\text{Ca}^{2+}]^{\text{CV}} \right) \right] + \frac{1}{2} \quad (17)$$

Calcium ions can be transported across the membrane up to an accumulation factor of 10^5 (Gussone et al., 2006).

$$\text{fun}_{\text{CaHCOH}}^{\text{HCO}_3^-} = \frac{1}{2} \cdot \tanh \left[1.5 \cdot \left([\text{HCO}_3^-]^{\text{CS}} - [\text{HCO}_3^-]^{\text{thresh}} \right) \right] + \frac{1}{2} \quad (18)$$

Cytosolic HCO_3^- is available for the $\text{Ca}^{2+}/\text{HCO}_3^-/\text{H}^+$ antiporter, when $[\text{HCO}_3^-]^{\text{CS}}$ exceeds $[\text{HCO}_3^-]^{\text{thresh}}$

$$\text{fun}_{\text{CaHCOH}}^{\text{ener}} = \max \left[\min \left(\frac{R_{\text{PS}} - R_{\text{PS, min}}}{R_{\text{PS, max}}}, 1 \right), 0 \right] \quad (19)$$

Energy equivalents can be provided via respirational processes. As respiration itself is not considered in this model (due to a lack of knowledge), we assume that POC production rates have to be high in order to provide the $\text{Ca}^{2+}/\text{HCO}_3^-/\text{H}^+$ antiporter with energy equivalents (**15** in Fig. 2). R_{PS} is the photosynthetic carbon fixation rate at prevailing light intensity (Eq. (22)).

2.2.6. Precipitation of calcium carbonate (**13** in Fig. 2)

Calcite is precipitated from Ca^{2+} and CO_3^{2-}



The corresponding precipitation rate (after Zuddas and Mucci, 1994) is

$$R_{\text{P}} = \begin{cases} k_f (\Omega - 1)^n & \text{for } \Omega > 1 \\ 0 & \text{for } \Omega \leq 1 \end{cases} \quad (21)$$

where Ω is the calcite saturation product that is dependent on the prevailing concentrations of Ca^{2+} and CO_3^{2-} (Mucci, 1983; Zeebe and Wolf-Gladrow, 2001). The parameter n is given in Zuddas and Mucci (1994), and k_f can be calculated (Zuddas and Mucci, 1994; Holtz et al., 2013a).

2.2.7. Photosynthetic carbon fixation (**14** in Fig. 2)

Carbon fixation by RubisCO depends on the CO_2 concentration within the thylakoid/pyrenoid complex

$$R_{\text{PS}} = \begin{cases} \frac{R_{\text{max}}^{\text{Rub}} \cdot [\text{CO}_2]^{\text{TP}}}{K_m^{\text{Rub}} + [\text{CO}_2]^{\text{TP}}} & \text{in the light} \\ 0 & \text{at darkness} \end{cases} \quad (22)$$

The maximum CO_2 fixation rate $R_{\text{max}}^{\text{Rub}}$ depends on the 'light-acclimation state' of the cell

$$R_{\text{max}}^{\text{Rub}} = \frac{L_{\text{CV}}}{V_{\text{TP}}} \cdot (10.67 \cdot \ln(I) - 21.85) \quad (23)$$

where I denotes the prevailing light intensity in $\mu\text{mol photons m}^{-2} \text{s}^{-1}$. L_{CV} is a conversion factor (Table 4). Eq. (23) is deduced from fitting the maximum net POC production rates (per hour of illumination) measured for different photon flux intensities (15, 80, 170, 200, and 400 $\mu\text{mol photons m}^{-2} \text{s}^{-1}$, cf. Fig. 3) by Zondervan et al. (2002)/Rost et al. (2002), Langer et al. (2009), and Hoppe et al. (2011). We generally use instantaneous net POC and PIC production rates here, i.e. we do not use rates integrated over the day that may include a dark phase.

2.2.8. Model equations

The numerical model consists of 23 coupled differential equations that describe the rates by which the concentrations of CO_2 , HCO_3^- , CO_3^{2-} , OH^- , H^+ (in all 4 compartments), Ca^{2+} and PIC (in CV), and POC (in TP) change. In the following, the differential equations are

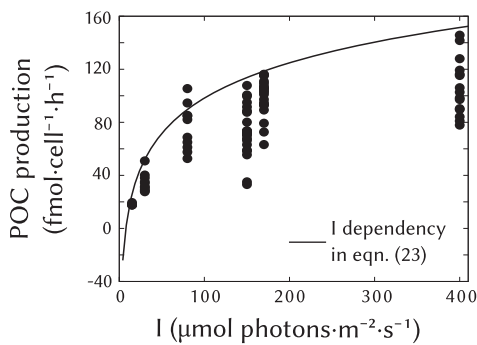


Fig. 3. Net particulate organic carbon (POC) production rates over irradiance levels (I) determined by Zondervan et al. (2002)/Rost et al. (2002), Langer et al. (2009), Hoppe et al. (2011), and Sett et al. (2014). The line indicates the implemented light dependency of RubisCO's maximum CO_2 fixation rate $R_{\text{max}}^{\text{Rub}}$ (cf. Eq. (23)).

listed according to their compartmental affiliation. Concentrations are given in mol m^{-3} and rates (R) in $\text{mol m}^{-3} \text{h}^{-1}$.

2.2.9. Cytosol (CS)

$$\begin{aligned} \begin{pmatrix} d[\text{CO}_2]^{CS}/dt \\ d[\text{HCO}_3^-]^{CS}/dt \\ d[\text{CO}_3^{2-}]^{CS}/dt \\ d[\text{H}^+]^{CS}/dt \\ d[\text{OH}^-]^{CS}/dt \end{pmatrix} &= \begin{pmatrix} R_1 + R_4 \\ -R_1 - R_4 - R_5^{\text{H}^+} + R_5^{\text{OH}^-} \\ R_5^{\text{H}^+} - R_5^{\text{OH}^-} \\ -R_1 + R_5^{\text{H}^+} - R_6 \\ R_4 + R_5^{\text{OH}^-} - R_6 \end{pmatrix} \\ &+ \begin{pmatrix} R_{\text{CO}_2, \text{PM}}^{CS} - R_{\text{CO}_2, \text{CVm}}^{CS} - R_{\text{CO}_2, \text{CPm}}^{CS} \\ R_{\text{HCO}_3^-, \text{PM}}^{CS} - R_{\text{CaHCOH, CVm}}^{CS} - R_{\text{HCO}_3^-, \text{CPm}}^{CS} \\ 0 \\ -R_{\text{H}^+, \text{PM}}^{CS} + R_{\text{CaHCOH, CVm}}^{CS} - R_{\text{H}^+, \text{CPm}}^{CS} \\ 0 \end{pmatrix} \end{aligned} \quad (24)$$

The carbonate system of the cytosol is described by the first set of parentheses on the right hand side (cf. Section 2.2.1). For the remaining three compartments (CV, CPs, and TP, cf. Sections 2.2.10–2.2.12), this description will be abbreviated by ‘C system’. Compartment-specific rates are listed in the second set of parentheses, where $R_{\text{CO}_2, \text{PM}}$ (cf. Eq. (11), **1** in Fig. 2) stands for the CO_2 , $R_{\text{HCO}_3^-, \text{PM}}$ (cf. Eq. (12), **2** and **3** in Fig. 2) for the HCO_3^- , and $R_{\text{H}^+, \text{PM}}$ (cf. Eq. (14), **4** in Fig. 2) for the H^+ flux across the plasma membrane. $R_{\text{CO}_2, \text{CVm}}$ (cf. Eq. (11), **5** in Fig. 2) gives the CO_2 flux and $R_{\text{CaHCOH, CVm}}$ (cf. Eq. (16), **6** in Fig. 2) the flux of Ca^{2+} , HCO_3^- , and H^+ across the CV membrane. $R_{\text{CO}_2, \text{CPm}}$ (cf. Eq. (11), **7** in Fig. 2), $R_{\text{H}^+, \text{CPm}}$ (cf. Eq. (14), **8** in Fig. 2), and $R_{\text{HCO}_3^-, \text{CPm}}$ (cf. Eq. (12), **9** in Fig. 2) denote the CO_2 , H^+ , and HCO_3^- fluxes across the chloroplast envelope.

2.2.10. Coccolith vesicle (CV)

$$\begin{aligned} \begin{pmatrix} d[\text{CO}_2]^{CV}/dt \\ d[\text{HCO}_3^-]^{CV}/dt \\ d[\text{CO}_3^{2-}]^{CV}/dt \\ d[\text{H}^+]^{CV}/dt \\ d[\text{OH}^-]^{CV}/dt \\ d[\text{Ca}^{2+}]^{CV}/dt \\ d[\text{PIC}]^{CV}/dt \end{pmatrix} &= \begin{pmatrix} \text{C system} \\ 0 \\ 0 \end{pmatrix} + \begin{pmatrix} R_{\text{CO}_2, \text{CVm}}^{CV} \\ R_{\text{CaHCOH, CVm}}^{CV} \\ -R_P \\ -R_{\text{CaHCOH, CVm}}^{CV} \\ 0 \\ R_{\text{CaHCOH, CVm}}^{CV} - R_P \\ R_P \end{pmatrix} \end{aligned} \quad (25)$$

where R_P stands for the precipitation rate of calcite (cf. Eq. (21), **13** in Fig. 2).

2.2.11. Chloroplast stroma (CPs)

$$\begin{aligned} \begin{pmatrix} d[\text{CO}_2]^{CPs}/dt \\ d[\text{HCO}_3^-]^{CPs}/dt \\ d[\text{CO}_3^{2-}]^{CPs}/dt \\ d[\text{H}^+]^{CPs}/dt \\ d[\text{OH}^-]^{CPs}/dt \end{pmatrix} &= \begin{pmatrix} \text{C system} \\ 0 \\ 0 \end{pmatrix} + \begin{pmatrix} R_{\text{CO}_2, \text{CPm}}^{CPs} - R_{\text{CO}_2, \text{TP}}^{CPs} \\ R_{\text{HCO}_3^-, \text{CPm}}^{CPs} - R_{\text{HCO}_3^-, \text{TP}}^{CPs} \\ 0 \\ R_{\text{H}^+, \text{CPm}}^{CPs} - R_{\text{H}^+, \text{TP}}^{CPs} \\ 0 \end{pmatrix} \end{aligned} \quad (26)$$

where the ‘C system’ includes CA activity (cf. Section 2.2.1). $R_{\text{HCO}_3^-, \text{TP}}$ (cf. Eq. (12), **10** in Fig. 2), $R_{\text{CO}_2, \text{TP}}$ (cf. Eq. (11), **11** in Fig. 2), and $R_{\text{H}^+, \text{TP}}$ (cf. Eq. (14), **12** in Fig. 2) indicate the fluxes of HCO_3^- , CO_2 , and H^+ between chloroplast stroma and thylakoid lumen.

2.2.12. Thylakoid/pyrenoid complex (TP)

$$\begin{aligned} \begin{pmatrix} d[\text{CO}_2]^{TP}/dt \\ d[\text{HCO}_3^-]^{TP}/dt \\ d[\text{CO}_3^{2-}]^{TP}/dt \\ d[\text{H}^+]^{TP}/dt \\ d[\text{OH}^-]^{TP}/dt \\ d[\text{POC}]^{TP}/dt \end{pmatrix} &= \begin{pmatrix} \text{C system} \\ 0 \end{pmatrix} + \begin{pmatrix} R_{\text{CO}_2, \text{TP}}^{TP} - R_{\text{PS}} \\ R_{\text{HCO}_3^-, \text{TP}}^{TP} \\ 0 \\ R_{\text{H}^+, \text{TP}}^{TP} \\ 0 \\ R_{\text{PS}} \end{pmatrix} \end{aligned} \quad (27)$$

where the ‘C system’ includes CA activity. R_{PS} gives the CO_2 fixation rate by RubisCO (cf. Eq. (22), **14** in Fig. 2).

3. Results

Model equations are integrated until steady state is obtained for 7 (external carbonate systems) \times 7 (light level) different model forcing combinations. Two different sets of carbonate systems were chosen (cf. Table 1) and one set of irradiance levels (15, 30, 80, 150, 200, 300, and 400 $\mu\text{mol photons m}^{-2} \text{s}^{-1}$). Both carbonate system sets are chosen so that external CO_2 concentrations range from 0.5 to 45 mmol m^{-3} , a range that covers CO_2 concentrations expected until year 2100. In one approach, the carbonate systems are varied via pH changes (‘carbonate systems 1’ in Table 1), while keeping DIC concentrations constant. Carbon dioxide and HCO_3^- concentrations thus increase with decreasing pH as in the data sets of Zondervan et al. (2002)/Rost et al. (2002), Langer et al. (2009), Hoppe et al. (2011), and Sett et al. (2014) (Fig. 4). In the second approach, the (out of equilibrium) carbonate systems (‘carbonate systems 2’ in Table 1) differ in CO_2 concentrations only, i.e. HCO_3^- and H^+ concentrations are set constant. The latter carbonate systems are used to investigate the influence of external HCO_3^- on the model outputs (cf. Table 1, right plots in Figs. 8 and 9). Light is provided 16 h per day.

The data that are described first (Zondervan et al., 2002/Rost et al., 2002; Langer et al., 2009; Hoppe et al., 2011; Sett et al., 2014) were conducted at CO_2 concentrations comparable to the model forcings (cf. Table 1). The light:dark cycle varied from 16:8 to 24:0. As described in Section 2.2.4, we do not take into account data that were conducted at pH values below 7.6.

3.1. Model outputs

Inter-conversion between CO_2 and HCO_3^- inside the cytosol as well as inside the CV is low, as are the uptake rates of CO_2 into the CV (Figs. 5 and 6). Thus, external CO_2 ends up primarily in POC; external HCO_3^- , in contrast, is used for both, POC and PIC

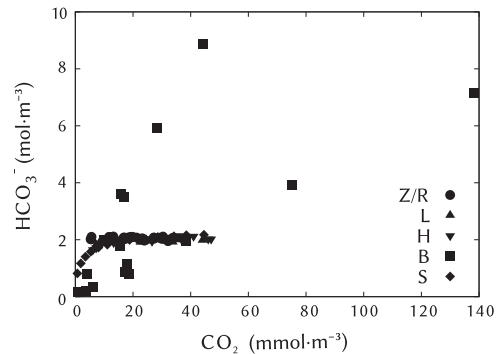


Fig. 4. Carbon dioxide and HCO_3^- concentrations used in the experiments of Zondervan et al. (2002)/Rost et al. (2002) (Z/R), Langer et al. (2009) (L), Hoppe et al. (2011) (H), Bach et al. (2013) (B), and Sett et al. (2014) (S). The HCO_3^- concentration is plotted against the CO_2 concentration. The decoupled carbonate systems used by Bach et al. (2013) cover a much wider range than those of the others.

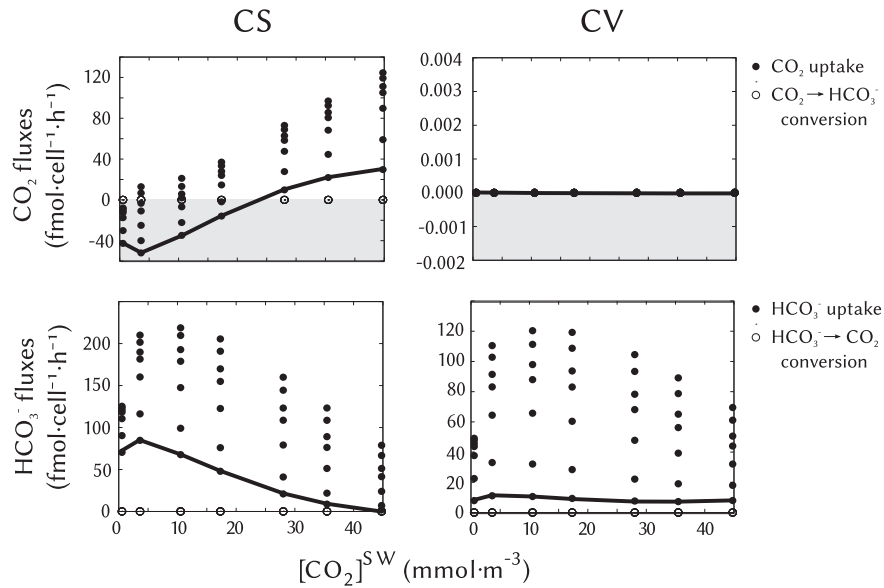


Fig. 5. Above: comparison between CO₂ uptake rates into the cell (CS, cytosol) and into the coccolith vesicle (CV) (filled circles) and CO₂ to HCO₃⁻ conversion rates within the cytosol and the CV (open symbols). All calculations were done for seven different light levels. Below: comparison between HCO₃⁻ uptake rates (filled circles) and HCO₃⁻ to CO₂ conversion rates (open symbols). Rates are plotted over external CO₂ concentration ([CO₂]^{SW}). Continuous lines indicate outputs generated at 15 μmol photons m⁻² s⁻¹. The calculated rates increase with light intensities. Calculations are based on carbonate systems 1 (cf. Table 1). Grey shaded areas indicate negative fluxes, i.e. release rates, not uptake rates.

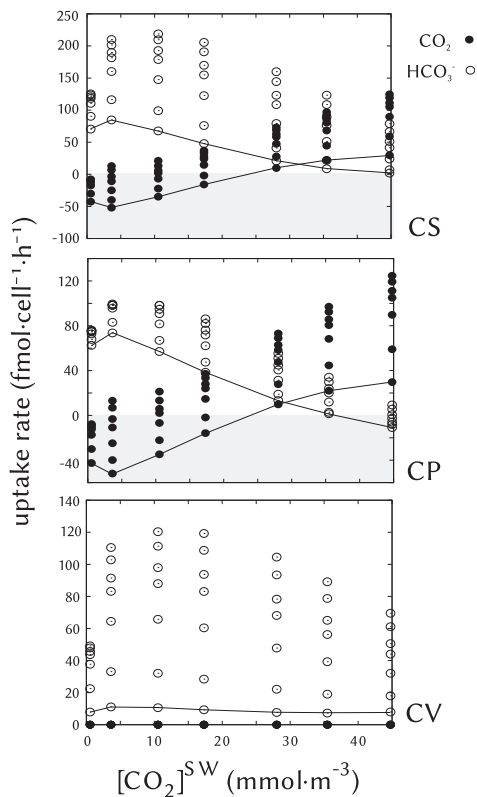


Fig. 6. Uptake rates of CO₂ (filled circles) and HCO₃⁻ (open circles) into the cell (CS, cytosol), the chloroplast (CP), and the coccolith vesicle (CV). Rates are plotted over external CO₂ concentration ([CO₂]^{SW}). Continuous lines indicate outputs generated at 15 μmol photons m⁻² s⁻¹. The calculated rates increase with light intensities. Calculations are based on carbonate systems 1 (cf. Table 1). Grey shaded areas indicate negative flux rates, i.e. release rates, not uptake rates.

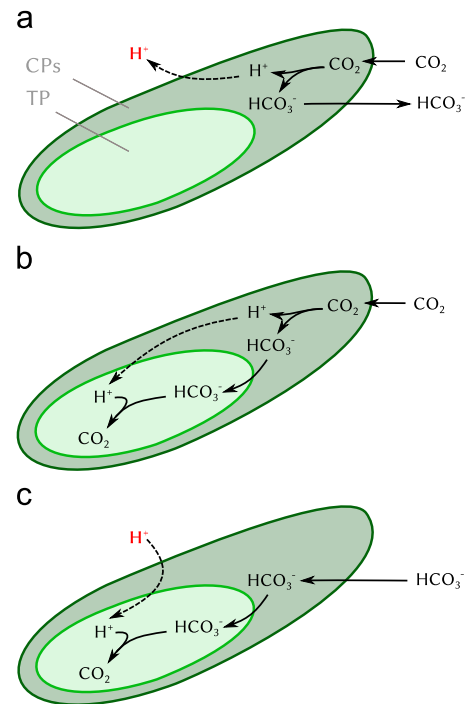


Fig. 7. Carbon flux related H⁺ budget of the chloroplast. (a) CO₂ is taken up and converted to HCO₃⁻ inside the chloroplast stroma (CPs) where carbonic anhydrase is active. HCO₃⁻ leaves the chloroplast again. The produced H⁺ has to be extruded from the chloroplast (against concentration gradient and across three membrane layers). TP, thylakoid/pyrenoid complex. (b) CO₂ usage of the chloroplast for photosynthetic carbon fixation does not lead to H⁺ production or consumption by the chloroplast. Nevertheless, H⁺ have to cross the thylakoid membrane which is effectuated by photosynthetic light reactions. (c) HCO₃⁻ usage requires H⁺ uptake. For the illustrated H⁺ budgets we assume that H⁺ release during O₂ generation, electron transport chain and ATP generation related H⁺ fluxes across the thylakoid membrane, and H⁺ fixation in the Calvin cycle are balanced. Other processes such as H⁺ fixation during nitrite reduction are neglected.

production. At high external CO₂ concentrations, however, some of the CO₂ that is taken up into the chloroplast leaves the chloroplast in the form of HCO₃⁻ (cf. Figs. 6 and 7(a)). This HCO₃⁻ is

subsequently taken up into the CV. It thus follows that at high external CO₂ concentrations, a small amount of PIC is built from external CO₂ in our model. At low external CO₂ concentrations, an

efflux of CO_2 out of the chloroplast and the cell is calculated. This CO_2 originally stems from external HCO_3^- that is taken up into the chloroplast. Highest CO_2 efflux rates are calculated at lowest light intensities. All trans-membrane fluxes and internal concentrations of CO_2 , HCO_3^- , and H^+ calculated on the basis of carbonate systems 1 (Table 1) are available as Supplemental material for all 49 forcing combinations (7 carbonate systems \times 7 light levels).

Calculated PIC and POC production rates as well as the PIC:POC ratios increase with light intensities (Fig. 8). While POC production rates increase with external CO_2 concentrations throughout the examined CO_2 range (Fig. 9), PIC production rates as well as the PIC:POC ratios increase with external CO_2 only until around 10 mmol m^{-3} and then decrease (left plots). The increasing trend of POC and PIC production rates under low CO_2 concentrations is not observed when external HCO_3^- concentrations are set constant (carbonate systems 2 in Table 1, right plots in Figs. 8 and 9). The calculated decrease in PIC production at high CO_2 concentrations results from the downregulation of cellular HCO_3^- uptake under 'photosynthetic CO_2 sufficiency'.

3.2. Model-data comparison

The interrelation between the PIC:POC ratio and the external CO_2 concentration measured by Zondervan et al. (2002)/Rost et al. (2002)

(strain PML B92/11) and Sett et al. (2014) (strain PML B92/11, at 15°C) at $150 \mu\text{mol photons m}^{-2} \text{ s}^{-1}$ is described well by the model (Fig. 10). Also in line with the data are the 'saturating behaviour' of POC production rates and the decrease in PIC production rates calculated at high external CO_2 concentrations (cf. Section 3.1). However, the decrease in POC production rates that was measured by Sett et al. (2014) is not reproduced by the model. The absolute rates of both production rates are slightly overestimated.

The data sets of Zondervan et al. (2002)/Rost et al. (2002), Langer et al. (2009), Hoppe et al. (2011), and Sett et al. (2014) show that PIC production rates increase with POC production rates (Fig. 11). Particulate inorganic carbon production rates conducted at CO_2 concentrations below 20 mmol m^{-3} increase faster with POC production rates than those conducted at external CO_2 concentrations above 20 mmol m^{-3} . This trend is reproduced by the model.

The experiments of Bach et al. (2013) (strain PML B92/11) were conducted at very wide ranges of CO_2 and HCO_3^- concentrations (cf. Fig. 4) and thus fall outside the forcing range. When forcing the model by the external CO_2 and HCO_3^- concentrations used by Bach et al. (2013) (cf. Supplemental material to Bach et al., 2013), the observed trends can be reproduced (Fig. 12, model modifications are listed in Table 5). In line with the data, the increase in POC and PIC production rates with external CO_2 concentrations occurs earlier in the high pH set-up than in the low pH set-up which is

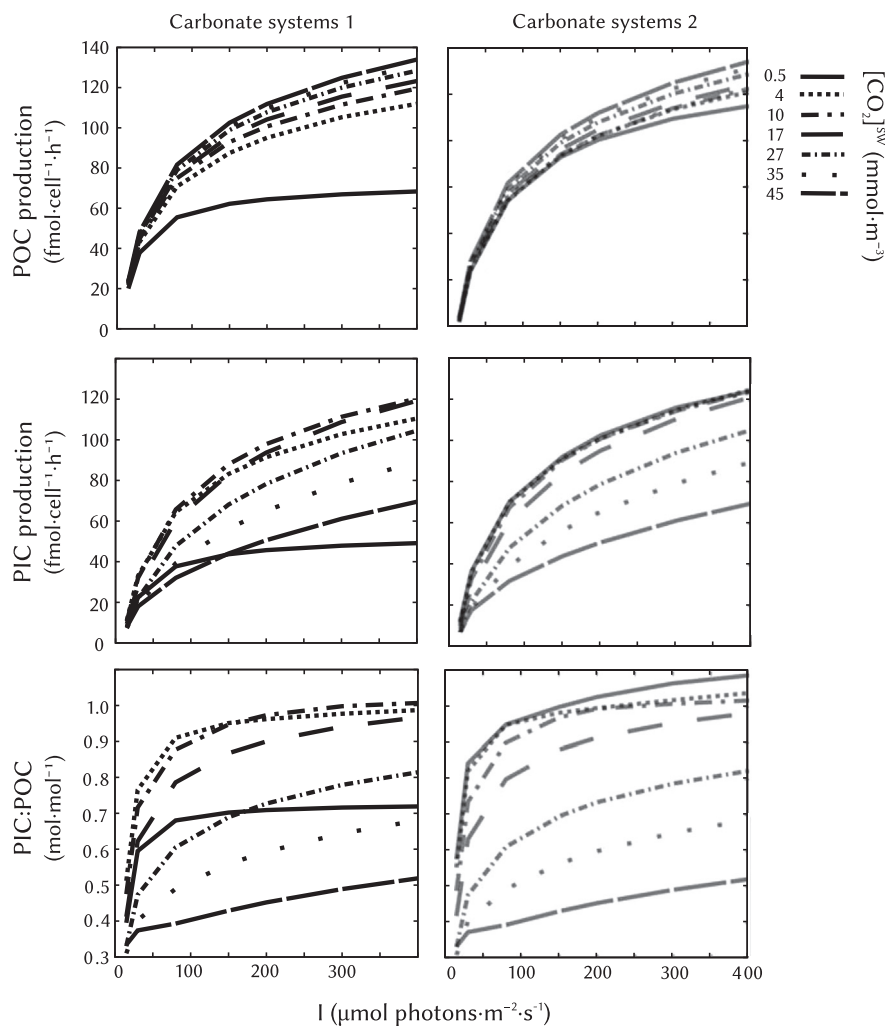


Fig. 8. Particulate organic and inorganic carbon (POC and PIC) production rates over light intensities (I) at 7 different external CO_2 concentrations $[\text{CO}_2]_{\text{SW}}^{\text{SW}}$. For reasons of breakdown, model outputs are interconnected by lines. Left: calculated on the basis of carbonate systems 1 (cf. Table 1). Right: calculated on the basis of the (out of equilibrium) carbonate systems 2 (cf. Table 1).

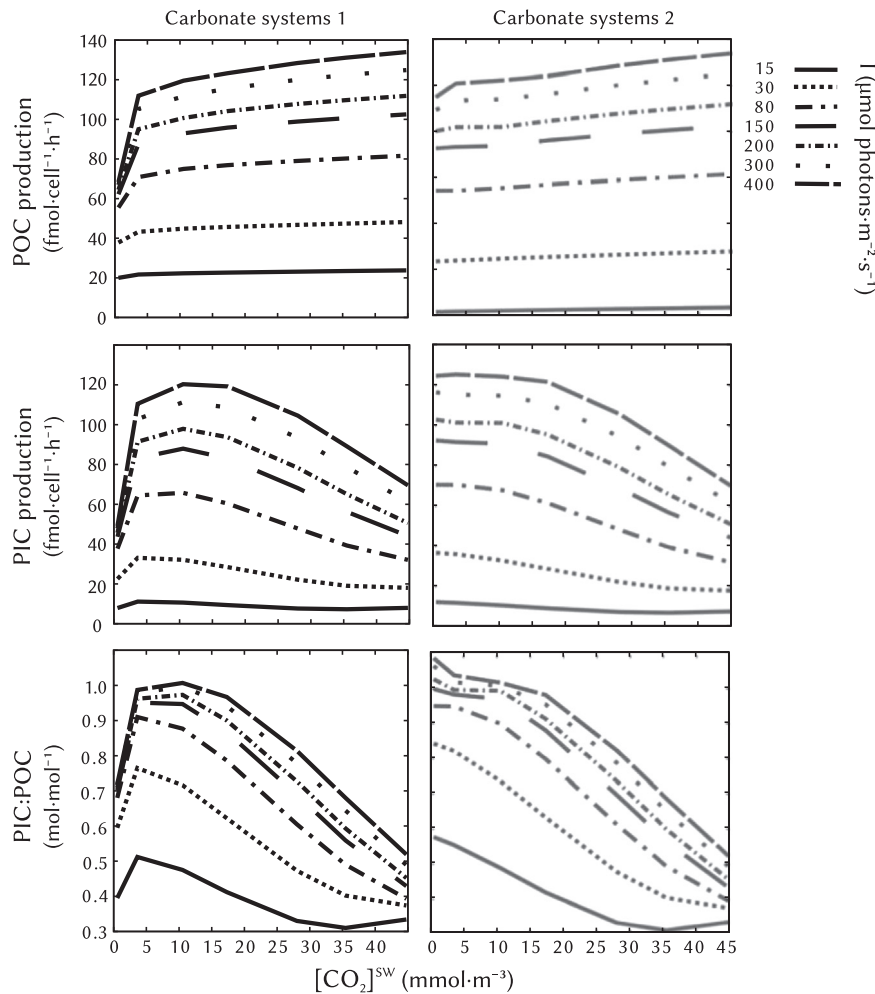


Fig. 9. Particulate organic and inorganic carbon (POC and PIC) production rates over external CO_2 concentrations at 7 different light intensities (I). For reasons of breakdown, model outputs are interconnected by lines. Left: calculated on the basis of carbonate systems 1 (cf. Table 1). Right: calculated on the basis of the (out of equilibrium) carbonate systems 2 (cf. Table 1).

due to the lower availability of external HCO_3^- under the latter conditions. We can thus show that this trend is not necessarily a pH effect. In contrast to our model outputs, Bach et al. (2013) measured a decrease in POC production rates (cf. data of Sett et al., 2014 in Fig. 11) with increasing DIC concentrations at high as well as at low pH values. Particulate organic carbon production rates at constant CO_2 concentrations are overestimated by the model. In case of PIC production rates, Bach et al. (2013) measure continuously high rates with rising CO_2 concentrations. Calculated PIC production rates are in line with this trend.

Examination of the *in silico* intracellular fluxes (Fig. 13) reveals that HCO_3^- constitutes the main carbon source for PIC and POC production at low external CO_2 concentrations, while at high CO_2 concentrations, CO_2 becomes more important. Under the latter conditions, HCO_3^- for PIC production is provided via the chloroplast in the model: CO_2 is converted to HCO_3^- inside the chloroplast stroma which then (partly) leaves the chloroplast into the cytosol following its concentration gradient. In order to support this pathway, we had to assume that diffusion out of the chloroplast can be faster than into it, i.e. that the electrical gradient of HCO_3^- across the chloroplast envelope directs out of the chloroplast (cf. Table 5). Above around 40 mmol m^{-3} , CO_2 becomes the dominant carbon source of POC production and an efflux of HCO_3^- out of the chloroplast is calculated for CO_2 concentrations exceeding 60 mmol m^{-3} .

3.3. Summary

- Significant intracellular CO_2 – HCO_3^- inter-conversion is calculated only within the chloroplast, where carbonic anhydrase is active.
- Depending on light levels and the carbonate system composition, CO_2 can enter or leave the cell via diffusion in our model. The efflux of CO_2 out of the cell results from chloroplast-internal HCO_3^- to CO_2 conversion.
- At low external CO_2 concentrations, measured PIC and POC production rates are low. Our model suggests that this effect may be caused by HCO_3^- limitation, not by CO_2 limitation.
- Our model explains the often observed decrease in PIC production rates under Ocean Acidification via a downregulation of cellular HCO_3^- uptake.
- In the data set of Bach et al. (2013), PIC production rates remain constant at high CO_2 concentrations. High calculated PIC production rates are provided with HCO_3^- via chloroplast-internal CO_2 to HCO_3^- conversion.
- The interrelation between PIC and POC production rates of different strains that are acclimated to different irradiance levels and carbonate systems is reproduced well by our model.
- The decrease in POC production rates at high DIC concentrations (Sett et al., 2014; Bach et al., 2013) is not reproduced by the model.

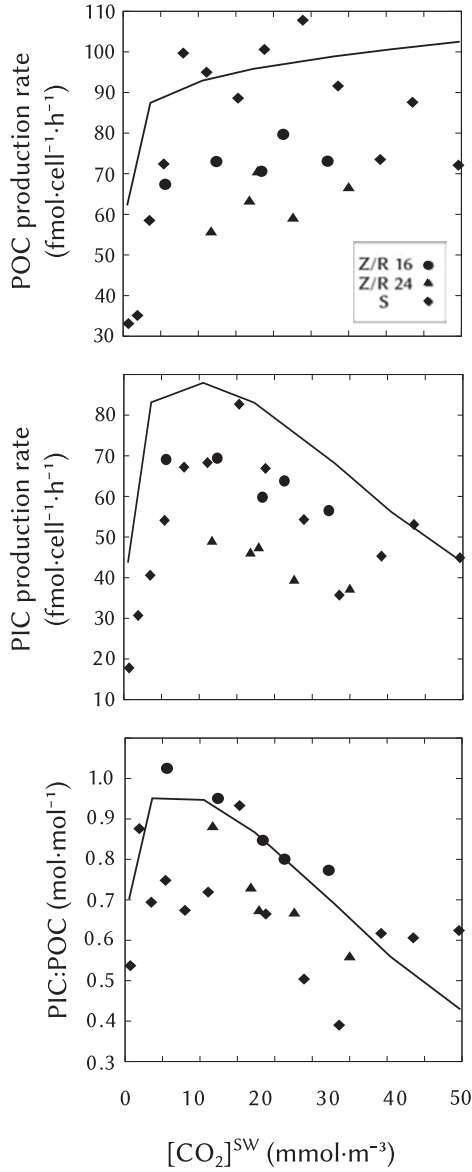


Fig. 10. Particulate organic and inorganic carbon (POC and PIC) production rates during illumination ($150 \mu\text{mol photons m}^{-2} \text{s}^{-1}$) and PIC:POC ratios over external CO_2 concentration. The data of Sett et al. (2014) and Zondervan et al. (2002)/Rost et al. (2002) are indicated by squared, round, and triangle symbols. S and Z/R 16 indicate data that were conducted at light:dark cycles of 16:8 h. Z/R 24 were conducted at 24 h of illumination. Data conducted at suboptimal temperatures or pH values < 7.6 are not accounted for. Model outputs are indicated by lines and are calculated on basis of carbonate systems 1 (cf. Table 1).

4. Discussion

Coccolithophores play an essential role in the marine carbon cycle. In order to predict their impact on the carbon cycle in the future oceans, it is crucial to understand the impact of abiotic conditions on cellular carbon fluxes. Many experiments have been conducted to examine this issue (for a summary see e.g. Raven and Crawford, 2012). Especially in terms of PIC production rates, results are partly contradictory. We here established a numerical cell model by means of which we are able to give a mechanistic explanation for several pattern observed under different acclimation conditions. In the following, our findings concerning the regulation of POC and PIC production are summarised (cf. Fig. 14).

POC production: Photosynthetic carbon fixation is strongly dependent on light and the CO_2 concentration around RubisCO.

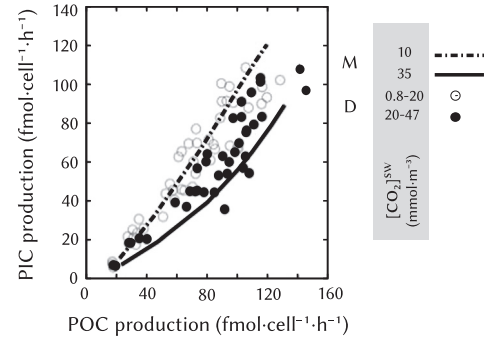


Fig. 11. Connectivity between PIC and POC production rates measured for strains PML B92/11, NZEH/PLY M219, RCC1212, RCC1216, RCC1238, and RCC1256 by Zondervan et al. (2002)/Rost et al. (2002), Langer et al. (2009), Hoppe et al. (2011), and Sett et al. (2014). Data represented by open and closed symbols were conducted at $[\text{CO}_2]$ below 20 mmol m^{-3} and above 20 mmol m^{-3} , respectively. The dotted and the solid line give the model outputs generated at an external $[\text{CO}_2]$ of 10 mmol m^{-3} and 35 mmol m^{-3} , respectively (light: $15\text{--}400 \mu\text{mol photons m}^{-2} \text{s}^{-1}$). Calculated on the basis of carbonate systems 1 (cf. Table 1). Data conducted at pH values below 7.6 or non-optimal growth temperatures are not plotted.

Table 5

Model modifications used to describe the experiment of Bach et al. (2013). (no.) is the process number given in Fig. 2. CPm, chloroplast envelope; CV, coccolith vesicle; I, light intensity in $\mu\text{mol photons m}^{-2} \text{s}^{-1}$, PM, plasma membrane; Rub, RubisCO.

Modification (no. in Fig. 2)

$$\gamma_{\text{HCO}_3^-}^{\text{PM},i} = 0.2 \text{ m h}^{-1} \quad (3)$$

$$[\text{HCO}_3^-]^{\text{thresh}} = 0.65 \text{ mol m}^{-3} \quad (6)$$

$$R_{\text{CaHCO}_3}^{\text{Ca}^{2+}} = 1.05 \times 10^{-13} \text{ mol h}^{-1} \quad (6)$$

$$\gamma_{\text{HCO}_3^-}^{\text{CPm}} = 51 \times 10^{-4} \text{ m h}^{-1} \quad (9)$$

$$R_{\text{HCO}_3^-}^{\text{CPs},\text{CPm}} = \gamma_{\text{HCO}_3^-}^{\text{CPm}} \cdot \frac{A^{\text{CP}}}{V_{\text{CPs}}} \cdot ([\text{HCO}_3^-]^{\text{CS}} - [\text{HCO}_3^-]^{\text{CPs}}) \quad (9)$$

$$R_{\text{HCO}_3^-}^{\text{CS},\text{CPm}} = 10 \cdot \gamma_{\text{HCO}_3^-}^{\text{CPm}} \cdot \frac{A^{\text{CP}}}{V_{\text{CS}}} \cdot ([\text{HCO}_3^-]^{\text{CPs}} - [\text{HCO}_3^-]^{\text{CS}}) \quad (9)$$

$$\gamma_{\text{HCO}_3^-}^{\text{TP}} = 0.01 \text{ m h}^{-1} \quad (10)$$

$$R_{\text{max}}^{\text{Rub}} = \frac{R_{\text{max}}^{\text{Rub}}(I=150)}{1.3} \quad (14)$$

$$\text{fun}_{\text{CaHCO}_3}^{\text{ener}} = \min \left[\max \left(0, \frac{R_{\text{PS}} - \frac{R_{\text{PSmin}}}{1.3}}{R_{\text{PSmax}}} \right), 1 \right] \quad (15)$$

We assume that light controls maximum carbon-fixation rates and that the upregulation of CO_2 around RubisCO is effected by an energy-efficient, chloroplast-based CCM. Carbon dioxide is assumed to be the preferred carbon source. In case diffusive uptake does not suffice to cover the carbon demand of photosynthesis, external HCO_3^- is used. The switch from CO_2 to HCO_3^- usage is achieved via an upregulation of anion exchangers in the plasma membrane (cf. Section 2.1). At very low external CO_2 concentrations, data show that POC production rates decrease (e.g. Fig. 10). In our model, this decrease results in particular from the lower external HCO_3^- concentrations at these conditions, but also – to a minor extent though – from CO_2 leakage out of the chloroplast (Fig. 6). At high external DIC concentrations, a decrease in POC production rates is observed that is not described by our model. In the data set of Bach et al. (2013) (Fig. 12), this decrease occurs at HCO_3^- concentrations above ca. 3000 mmol m^{-3} – independently of pH and CO_2 concentration. At such high HCO_3^- concentrations, strong chemical potential differences of HCO_3^- across the plasma membrane may support fast HCO_3^- influx rates into the cell. While PIC production rates seem to benefit (slightly though) from the additional HCO_3^- provision, POC production rates decrease. Since (net) POC production rates basically give the difference between photosynthetic CO_2 fixation and respiratory loss, the observed decrease in POC may either result from

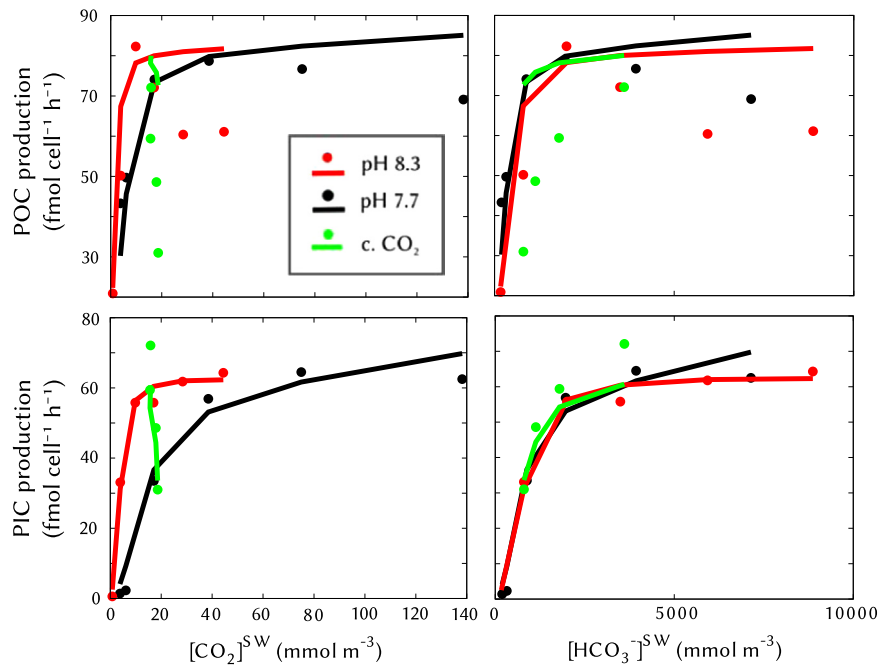


Fig. 12. Particulate inorganic and organic carbon (PIC and POC, respectively) production rates measured by Bach et al. (2013) (filled circles). Data conducted at low pH values (7.7) are illustrated in black, those conducted at high pH values (8.3) are given in red colours, and data that were conducted at constant CO_2 concentrations are given in green colours. Model outputs are illustrated by lines. Data points conducted at pH values below 7.6 were not taken into account. (For interpretation of the references to color in this figure caption, the reader is referred to the web version of this paper.)

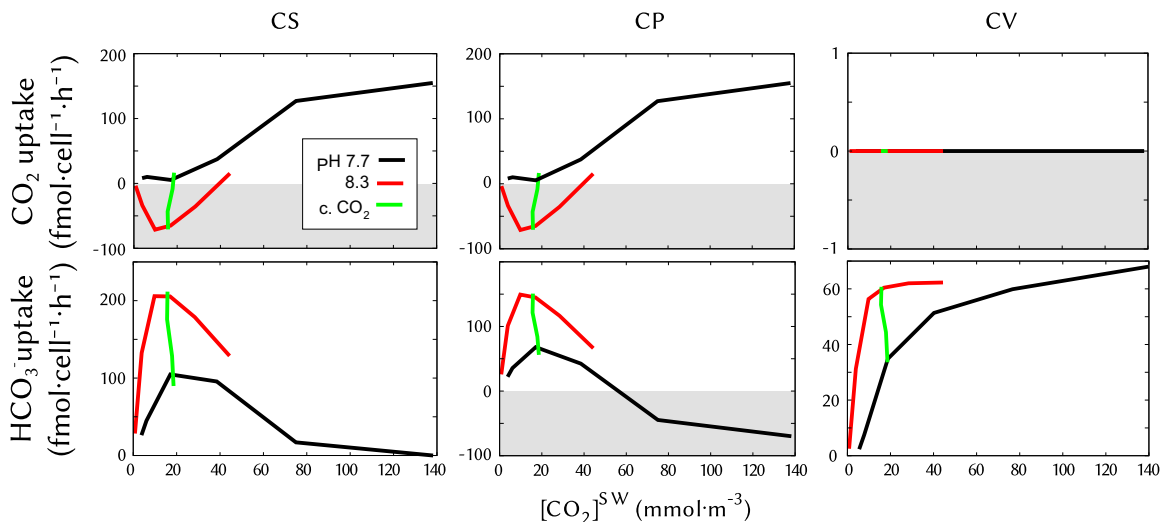


Fig. 13. Calculated CO_2 and HCO_3^- fluxes into the cytosol (CS), the chloroplast (CP), and the coccolith vesicle (CV) to the data of Bach et al. (2013) (cf. Fig. 12). Positive values indicate fluxes into cytosol, chloroplast, and CV; negative values indicate an efflux. Black lines – pH 7.7, red lines – pH 8.3, green lines – constant CO_2 . Grey shaded areas indicate negative fluxes, i.e. effluxes. (For interpretation of the references to color in this figure caption, the reader is referred to the web version of this paper.)

lowered CO_2 fixation rates or rising respiration rates. Rising respiration rates may for instance be caused by high energy demands associated with increasing HCO_3^- influx rates (cf. Section 2.1). The decrease in CO_2 fixation rates, on the other hand, may be induced for instance by a weakened pH gradient across the thylakoid membrane (cf. Fig. 7(c)), resulting from thylakoid-internal HCO_3^- to CO_2 conversion rates that exceed the required H^+ delivery flux. A similar indirect pH effect may occur when chloroplast-internal CO_2 to HCO_3^- conversion rates that support PIC production (cf. Fig. 7(a)) are high. While it is not possible to clarify this issue finally, we can conclude that the observed model-data discrepancy at high DIC concentrations does not contradict the general model set-up.

PIC production: Calcite is precipitated inside the CV, in which the calcite saturation product Ω is upregulated via active transport processes. These transport processes are driven by respiratory processes that are dependent on high photosynthetic carbon fixation rates in our model. Bicarbonate and Ca^{2+} are taken up into the CV in antiport against H^+ . The Ca^{2+} concentration inside the cytosol is known to be strictly regulated and thus set to a constant low value in our model. The cytosolic HCO_3^- concentration, in contrast, is variable. We assume that cellular HCO_3^- uptake is upregulated when the carbon demand of photosynthesis cannot be covered by CO_2 diffusion. The calculated decrease in PIC production rates at very low external CO_2 concentrations that is in line with observations thus results from the decrease in external HCO_3^- concentrations. The efflux of CO_2 from

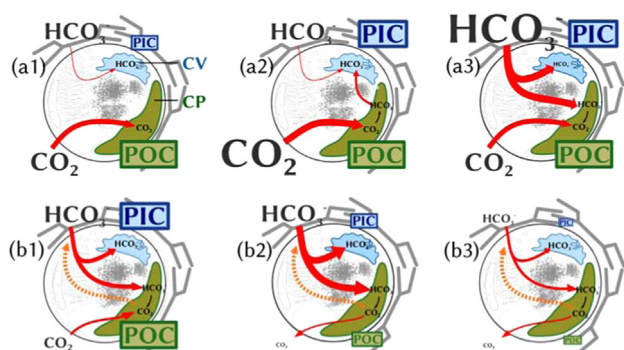


Fig. 14. Principle pattern for the distribution of dissolved inorganic carbon fluxes at different external carbonate system compositions. (a1) High $[CO_2]$ and medium $[HCO_3^-]$: CO_2 is taken up into the chloroplast (CP) via diffusion. Low HCO_3^- uptake rates lead to low particulate inorganic carbon (PIC) production rates. From here (a1), either external CO_2 (a2) or HCO_3^- (a3) is increased. (a2) Increase in $[CO_2]$: CO_2 enters the chloroplast, is converted to HCO_3^- , leaves the chloroplast, and enters the cocolith vesicle (CV). PIC production increases. Whether this pathway exists depends on the capacity of HCO_3^- to leave the chloroplast. (a3) Increase in $[HCO_3^-]$: although HCO_3^- uptake capacity of the plasma membrane is low, HCO_3^- uptake increases due to high external $[HCO_3^-]$. PIC production increases. (b1) Medium $[CO_2]$ and medium $[HCO_3^-]$ (cf. e.g. outputs to $[CO_2] = 17 \text{ mmol m}^{-3}$ and $I = 80 \mu\text{mol photons m}^{-2} \text{ s}^{-1}$, Supplemental material): when the $[CO_2]$ around RubisCO falls below a critical threshold, cellular HCO_3^- uptake is upregulated (orange-dotted arrow). CP and CV take up HCO_3^- . PIC and POC production rates are high. From here (b1), first external $[CO_2]$ is reduced (b2), then external $[CO_2]$ and $[HCO_3^-]$ (b3). (b2) Decrease in $[CO_2]$ (cf. e.g. outputs to $[CO_2] = 0.5 \text{ mmol m}^{-3}$ and $I = 80 \mu\text{mol photons m}^{-2} \text{ s}^{-1}$, Supplemental material): CO_2 leaves the chloroplast following its concentration gradient and net POC production decreases. Less energy may be provided to carbon (and Ca^{2+}) uptake into the CV. Thus, PIC production rates may decrease also. This effect is of minor importance in our model. (b3) Decrease in $[CO_2]$ and $[HCO_3^-]$ (cf. e.g. Bach et al., 2013, pH 8.3, very low DIC): HCO_3^- uptake is low due to low external $[HCO_3^-]$. PIC and POC production rates decrease further. Illustration includes part that was redrawn after van der Wal et al. (1983). (For interpretation of the references to color in this figure caption, the reader is referred to the web version of this paper.)

the chloroplast which may imply a reduced energy availability for the $Ca^{2+}/HCO_3^-/H^+$ transporter of the CV (*in vivo* further energy-requiring processes are of course involved in calcite precipitation (summary e.g. in Holtz et al., 2013b)) is of minor importance, at least in our model. In case CO_2 diffusion can cover the carbon demand of photosynthesis, we assume low cellular HCO_3^- uptake and therewith a low HCO_3^- supply to the CV. This is our explanation for the low PIC production rates often observed at high CO_2 concentrations (e.g. Raven and Crawford, 2012). The PIC production rates measured by Bach et al. (2013) (decoupled carbonate system that covers a very wide range of $[CO_2]$ and $[HCO_3^-]$), however, remain constant at high CO_2 concentrations. Our model explains this pattern in the following: External CO_2 enters the chloroplast and is converted to HCO_3^- (driven by the high pH inside the chloroplast stroma and accelerated by CA activity). This HCO_3^- partly leaves the chloroplast via channel proteins that admit in – as well as effluxes. Once arrived within the cytosol, HCO_3^- can be imported into the CV and feed PIC production. This pathway may explain why the ^{13}C content of PIC in cocolithophores decreases at high external CO_2 concentrations (cf. Bolton and Stoll, 2013). In order to judge the influence of this hypothetical pathway on PIC production rates, however, more research is needed. Until now, not much is known, neither about the transport systems directly involved in calcification and photosynthesis in cocolithophores nor about their capacities or the intracellular distribution of electrochemical gradients.

To sum up, the established model is able to give a new mechanistic explanation for several pattern in PIC and POC production rates reported in the literature. The decrease in PIC production rates, for instance, that is usually observed under Ocean Acidification may well be induced by the increase in CO_2 concentration and not the decrease in pH. We further found that increasing light intensities, i.e. higher

photosynthetic carbon fixation rates, may upregulate cellular HCO_3^- uptake and therewith PIC production rates and hence PIC:POC ratios.

5. Conclusion

Based on experimental evidence, a new concept was developed that describes the regulation of cellular carbon fluxes in response to changing carbonate system compositions and irradiance levels. Internal pH homeostasis is presumed to be warranted. The concept was implemented into a numerical model that is able to reproduce PIC and POC production rates measured for different strains of *E. huxleyi* under different acclimation conditions. The model therewith gives a mechanistic explanation for the interrelation between carbonate system, irradiance level, and PIC and POC production rates.

Acknowledgements

We thank Dorothee Kottmeier and Björn Rost for helpful discussions and comments on the manuscript. Furthermore, we sincerely thank two anonymous reviewers for critically reading the paper. Their comments helped to improve and clarify the paper. L.-M. H. was funded by the Federal Ministry of Education and Research (BMBF, project ZeBiCa²).

Appendix A. Supplementary data

Supplementary data associated with this paper can be found in the online version at <http://dx.doi.org/10.1016/j.jtbi.2015.02.024>.

References

- Anning, T., Nimer, M., Merrett, M.J., Brownlee, C., 1996. Costs and benefits of calcification in cocolithophorids. *J. Mar. Syst.* 9, 45–56.
- Armstrong, R.A., Lee, C., Hedges, J.L., Honjo, S., Wakeham, S.G., 2002. A new, mechanistic model for organic carbon fluxes in the ocean based on the quantitative association of POC with ballast minerals. *Deep Sea Res. Part II* 49 (1–3), 219–236.
- Bach, L.T., Riebesell, U., Schulz, K.G., 2013. Dissecting the impact of CO_2 and pH on the mechanisms of photosynthesis and calcification in the cocolithophore *Emiliania huxleyi*. *New Phytol.* 5, 1–14. <http://dx.doi.org/10.1111/nph.12225>.
- Berridge, M.J., Lipp, P., Bootman, M.D., 2000. The versatility and universality of calcium signalling. *Nat. Rev.* 1, 11–21.
- Boller, A., Phaedra, J., Cavanaugh, C., Scott, K., 2011. Low stable carbon isotope fractionation by cocolithophore RubisCO. *Geochim. Cosmochim. Acta* 75, 7200–7207.
- Bolton, C.T., Stoll, H.M., 2013. Late Miocene threshold response of marine algae to carbon dioxide limitation. *Nature* 500, 558–562.
- Brownlee, C., Davies, M., Nimer, N., Dong, L.F., Merrett, M.J., 1995. Calcification, photosynthesis and intracellular regulation in *Emiliania huxleyi*. *Bull. Inst. Oceanograph.* 14, 19–35.
- Field, C.B., Behrenfeld, M.J., Randerson, J.T., Falkowski, P., 1998. Primary production of the biosphere: integrating terrestrial and oceanic components. *Science* 281, 237–240.
- Gouaux, E., MacKinnon, R., 2005. Principles of selective ion transport in channels and pumps. *Science* 310, 1461–1465.
- Gussone, N., Langer, G., Thoms, S., Nehrke, G., Eisenhauer, A., Riebesell, U., Wefer, G., 2006. Cellular calcium pathways and isotope fractionation in *Emiliania huxleyi*. *Geology* 34, 625–628.
- Heldt, H.W., Werdan, K., Milovancev, M., Geller, G., 1973. Alkalinization of the chloroplast stroma caused by light-dependent proton flux into the thylakoid space. *Biochim. Biophys. Acta* 314, 224–241.
- Holtz, L.-M., Thoms, S., Langer, G., Wolf-Gladrow, D.A., 2013a. Substrate supply for calcite precipitation in *Emiliania huxleyi*: assessment of different model approaches. *J. Phycol.* 49, 417–426.
- Holtz, L.-M., Langer, G., Rokitta, S.D., Thoms, S., 2013b. Synthesis of nanostructured calcite particles in cocolithophores, unicellular algae. In: Rai, M., Posten, C. (Eds.), *Green Biosynthesis of Nanoparticles—Mechanisms and Applications*. pp. 132–147. (www.cabi.org).
- Holtz, L.-M., Thoms, S., Wolf-Gladrow, D.A., 2015. Numerical cell model investigating cellular carbon fluxes in *Emiliania huxleyi*. *J. Theoret. Biol.* 364, 305–315. <http://dx.doi.org/10.1016/j.jtbi.2014.08.040>.

- Hopkinson, B.M., Dupont, C.L., Allen, A.E., Morel, F.M.M., 2011. Efficiency of the CO₂-concentrating mechanism of diatoms. *Proc. Natl. Acad. Sci. USA* 108 (10), 3830–3837.
- Hoppe, C., Langer, G., Rost, B., 2011. *Emiliana huxleyi* shows identical responses to elevated pCO₂ in TA and DIC manipulations. *J. Exp. Mar. Biol. Ecol.* 406, 54–62.
- Kottmeier, D.M., Rokitta, S.D., Tortell, P.D., Rost, B. Strong shift from CO₂ to HCO₃⁻ uptake in *Emiliana huxleyi* with acidification: new approach unravels acclimation versus short-term pH effects. *Photosynth. Res. Spec. Iss. CCM8* 121, 2014, 265–275. <http://dx.doi.org/10.1007/s11120-014-9984-9>.
- Langer, G., Nehrke, G., Probert, I., Ly, J., Ziveri, P., 2009. Strain-specific responses of *Emiliana huxleyi* to changing seawater carbonate chemistry. *Biogeosci. Discuss.* 6, 4361–4383.
- Milliman, J.D., 1993. Production and accumulation of calcium carbonate in the Ocean: Budget of a nonsteady state. *Global Biochem. Cycles* 7 (4), 927–957.
- Mucci, A., 1983. The solubility of calcite and aragonite in seawater at various salinities, temperatures, and one atmosphere total pressure. *Am. J. Sci.* 283, 780–799.
- Paasche, E., 2002. A review of the coccolithophorid *Emiliana huxleyi* (Prymnesiophyceae), with particular reference to growth, coccolith formation, and calcification-photosynthesis interactions. *Phycologia* 40 (6), 503–529, ISSN 0031-8884.
- Peters, G.P., Marland, G., Le Quéré, C., Boden, T., Canadell, J.G., Raupach, M.R., 2011. Rapid growth in CO₂ emissions after the 2008–2009 global financial crisis. *Nat. Clim. Change* 2, 2–4.
- Poulton, A.J., Adeya, T.R., Balch, W.M., Holligan, P.M., 2007. Relating coccolithophore calcification rates to phytoplankton community dynamics: regional differences and implications for carbon export. *Deep-Sea Res. II* 54, 538–557.
- Prasad, G.V.R., Coury, L.A., Finn, F., Zeidel, M.L., 1998. Reconstituted aquaporin 1 water channels transport CO₂ across membranes. *J. Biol. Chem.* 273 (50), 33123–33126.
- Raven, J.A., Crawford, K., 2012. Environmental controls on coccolithophore calcification. *Mar. Ecol. Prog. Ser.* 470, 137–166.
- Rost, B., Zondervan, I., Riebesell, U., 2002. Light-dependent carbon isotope fractionation in the coccolithophorid *Emiliana huxleyi*. *Limnol. Oceanogr.* 47 (1), 120–128.
- Rouco, M., Branson, O., Lebrato, M., Iglesias-Rodriguez, M.D., 2013. The effect of nitrate and phosphate availability on *Emiliana huxleyi* (NZEH) physiology under different CO₂ scenarios. *Front. Microbiol.* 1–11. <http://dx.doi.org/10.3389/fmicb.2013.00155>.
- Schmidt, K., De La Rocha, C.L., Gallinari, M., Cortese, G., 2014. Not all calcite ballast is created equal: differing effects of foraminiferan and coccolith calcite on the formation and sinking of aggregates. *Biogeosciences* 11 (135), 135–145.
- Sett, S., Bach, L.T., Schulz, K.G., Koch-Klavsen, S., Lebrato, M., Riebesell, U., 2014. Temperature modulates coccolithophorid sensitivity of growth, photosynthesis and calcification to increasing seawater pCO₂. *PLOS One* 9 (2), e88308. <http://dx.doi.org/10.1371/journal.pone.0088308>.
- Solomon, S., Qin, D., Manning, M., Chen, Z., Marquis, M., Averyt, K.B., Tignor, M., Miller, H.L., 2007. Contribution of Working Group I to the Fourth Assessment Report of the Intergovernmental Panel on Climate Change. Cambridge University Press, Cambridge (UK), New York (USA) 987.
- Supuran, C.T., Scozzafava, A., 2007. Carbonic anhydrases as targets for medicinal chemistry. *Bioorg. Med. Chem.* 15, 4336–4350.
- Thoms, S., Pahlow, M., Wolf-Gladrow, D.A., 2001. Model of the carbon concentrating mechanism in chloroplasts of eukaryotic algae. *J. Theoret. Biol.* 208, 295–313, ISSN 0022-5193.
- Uehlein, N., Otto, B., Hanson, D.T., Fischer, M., McDowell, N., Kaldenhoff, R., 2008. Function of *Nicotiana tabacum* aquaporins as chloroplast gas pores challenges the concept of membrane CO₂ permeability. *Plant Cell* 20, 648–657.
- van der Wal, P., de Jong, E., Westbroek, P., de Bruijn, W., Mulder-Stapel, A., 1983. Ultrastructural polysaccharide localization in calcifying and naked cells of the coccolithophorid *Emiliana huxleyi*. *Protoplasma* 118, 157–168, ISSN 0033-183X.
- Wolf-Gladrow, D.A., Zeebe, R.E., Klaas, C., Körtzinger, A., Dickson, A.G., 2007. Total alkalinity: the explicit conservative expression and its application to biogeochemical processes. *Mar. Chem.* 106, 287–300.
- Zeebe, R.E., Wolf-Gladrow, D.A., 2001. CO₂ in Seawater: Equilibrium, Kinetics, Isotopes. Elsevier Science Ltd, Amsterdam, ISBN 0444505792.
- Zondervan, I., Rost, B., Riebesell, U., 2002. Effect of CO₂ concentration on the PIC/POC ratio in the coccolithophore *Emiliana huxleyi* grown under light-limiting conditions and different daylengths. *J. Exp. Mar. Biol. Ecol.* 272, 55–70.
- Zuddas, P., Mucci, A., 1994. Kinetics of calcite precipitation from seawater: I. A classical chemical kinetics description for strong electrolyte solutions. *Geochim. Cosmochim. Acta* 58 (20), 4353–4362.